NASA-CR-194260

MCAT Institute
Final Report
93-18

Numerical Simulation of a Powered-Lift Landing, Tracking Flow Features Using Overset Grids, and Simulation of High Lift Devices on a Fighter-Lift-And-Control Wing

Kalpana Chawla

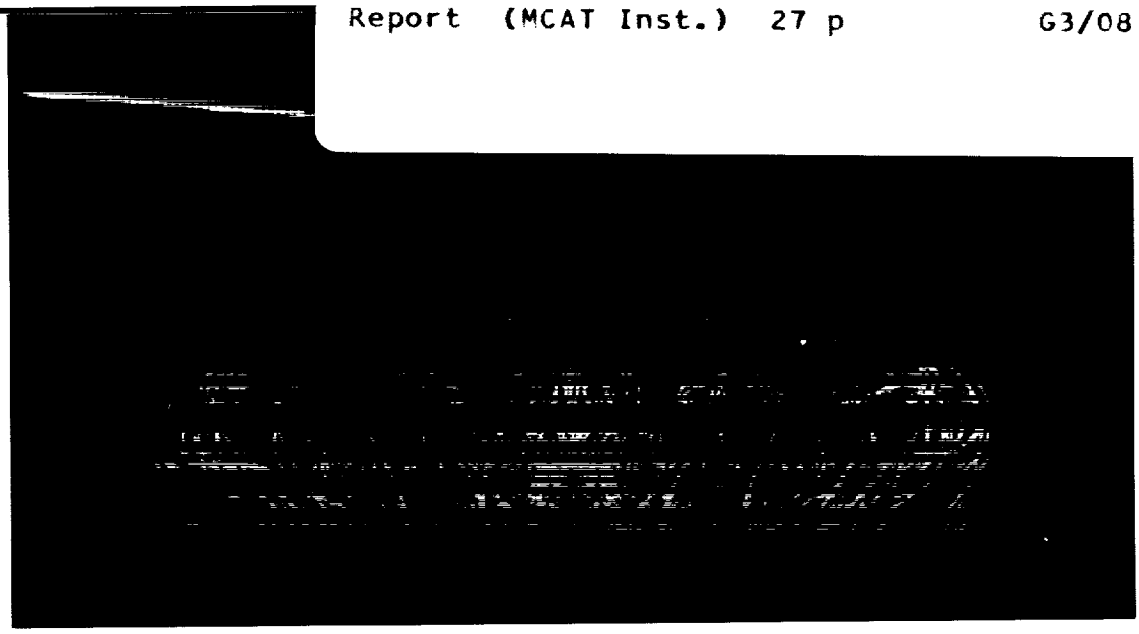

August 1993

NCC2-563

MCAT Institute
3933 Blue Gum Drive
San Jose, CA 95127

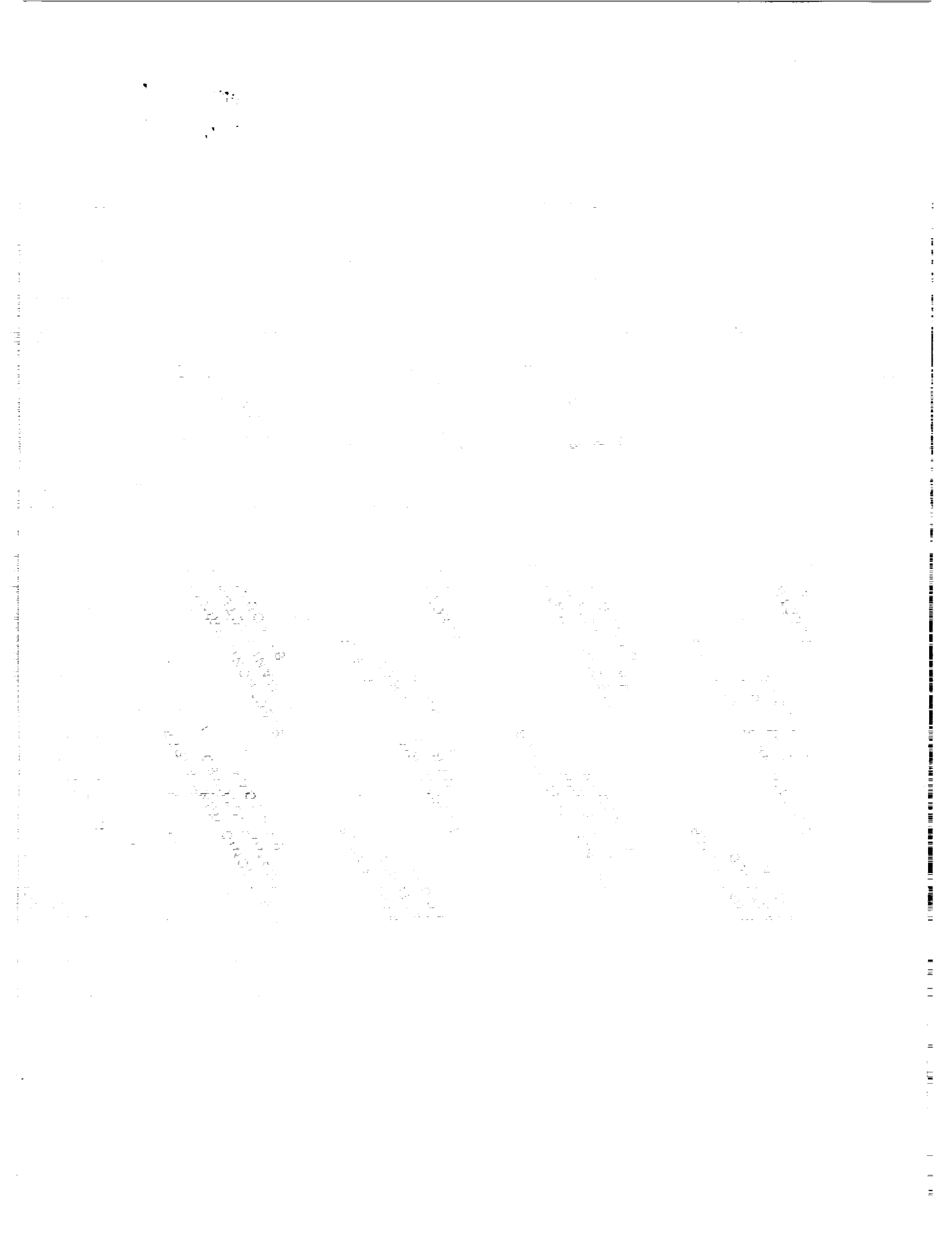

Final Report

Numerical Simulation of a Powered-Lift Landing, Tracking Flow Features Using Overset Grids, and Simulation of High Lift Devices on a Fighter- Lift-And-Control Wing

Kalpana Chawla

The work performed under grant NCC2-563 in the time period September 1992 to August 1993 included finishing the simulation of a landing powered-lift delta wing; tracking flow features using overset grids; and simulating flaps on the FLAC wing.

Within the first project, flow simulation was performed for a landing delta wing with thrust reverser jets starting from a height of one wing span above the ground and ending at a one-quarter of a wing span above the ground. The simulation captures the initial increased lift due to conventional ground cushion effect as the delta wing approaches the ground. The computed lift coefficients are over-predicted; however, the simulation can capture at least the qualitative trends in lift-loss encountered by thrust-vectoring aircraft operating in ground effect. Power spectra of temporal variations of pressure indicate that computed vortex shedding frequencies close to the jet exit are in the experimentally observed frequency range. Additionally, power spectra of temporal variations of pressure have provided insights into the mechanisms of lift oscillations. The detailed results of this work are included in Appendix I.

The second project dealt with tracking of dynamic flow features. Features of interest such as moving shock waves and vortices are overset with relatively fine tracker grids.

Solutions are computed on the various grids and information is exchanged at intergrid boundaries. A grid track-sensor variable such as pressure is used to track the position of the flow feature to be resolved. The tracker grid is moved to the position where the track-sensor variable has the desired value (generally a maximum or a minimum) and new interpolation coefficients are computed for information exchange across grid boundaries. Solutions are computed at the current location and time-step, and grid motion is brought into the solution via time metrics. The method is demonstrated by tracking a moving shock and vortices shed behind a circular cylinder. It is conjectured that the method would show significant benefits in resolving features such as wakes behind oscillating airfoils and trajectories of jets issuing from rotating nozzles as encountered during thrust-vectoring. The results of this work are included in Appendix II.

Finally, under the same grant, Chimera gridding strategies were devised to resolve narrow gaps between the control surfaces and the adjacent surfaces for Wright Patterson Lab's FLAC wing. Flow field simulations are in progress for various leading and trailing edge flap deflection angles. Appendix III shows surface grids for the FLAC wing and pressure coefficient contours for a Mach no. of 0.18 and Reynolds no. of 2.5 million.

Appendix I

N15

AGARD

72nd Fluid Dynamics Panel Meeting
and
Symposium
on
Computational and Experimental Assessment of Jets in Cross Flow

Winchester, United Kingdom, April 19-23, 1993

Numerical Simulation of a Powered-Lift Landing

by

Kalpana Chawla
MCAT Institute, M.S. 258-1
NASA Ames Research Center

and

William R. Van Dalsem
M.S. T045-2
NASA Ames Research Center
Moffett Field, CA 94035

Numerical Simulation of a Powered-Lift Landing

Kalpana Chawla
MCAT Institute
M.S. 258-1, NASA Ames Research Center
and
William R. Van Dalsem
M.S. T045-2, NASA Ames Research Center
Moffett Field, California 94035-1000
U.S.A

1. SUMMARY

The flow field about a delta wing equipped with thrust reverser jets in slow speed flight near the ground has been computed. Results include the prediction of the flow about the delta wing at four fixed heights above the ground, and a simulated landing, in which the delta wing descends towards the ground. Comparison of computed and experimental lift coefficients indicates that the simulations can capture at least the qualitiative trends in lift-loss encountered by thrust-vectoring aircraft operating in ground effect.

2. INTRODUCTION

Thrust vectoring can be used to improve short field, up-and-away, and post-stall maneuvering performance of high-performance aircraft. When vectored thrust is used to meet short runway requirements, as in the case of the Harrier AV-8B, a complex fluid dynamics interaction between the vectored jets, the ground, and the airframe is encountered. This flow field can put the aircraft at risk due to lift loss and hot-gas/debris ingestion. As a result of these risks, operational flexibility and performance may be reduced. Experiments performed by Paulson and Kemmerly[1] at NASA Langley's Vortex Research Facility (VRF) indicate that for a STOVL (Short Take-Off and Vertical Landing) configuration the magnitude of the loss in wing-borne lift is a strong function of its rate of descent. Although this phenomenon is not fully understood, it is known that during a landing with a rapid rate of descent, the lift loss is much less than in the case of a low (or zero) rate of descent. It is conjectured that at rapid rates of descent, insufficient time exists for the complete ground vortex structure to form under the aircraft. A computational study has been carried out to predict the lift-loss experienced by aircraft using thrust-vectoring in ground effect, and to understand the differences in flow physics in the straight-and-level flight and the descent cases.

To understand the jet related flow physics of the suck-down phenomenon, Van Dalsem[2,3] conducted a numerical study of the impingement of an unsteady three-dimensional jet on a ground plane, in cross-flow, by solution of the Reynolds-averaged Navier-Stokes equations. This work simulated the experimental work of Stewart, Kuhn and Walters.[4] Insights into the impinging jet flow physics, for example, the sensitivity of ground vortex location to the level of mixing in the wall jet were obtained in this work.[3] Also the computed ground vortex locations and the pressure coefficient distribution compared well with the experimental data. This effort quantified the ability of Computational Fluid Dynamics (CFD) to predict the strength and location of the primary features of the impinging jet flow-field.

To understand the suck-down effect, it was required to introduce an airframe in the above study, so that the interaction of the jets with the ground and the airframe could be studied. To concentrate resources on resolving the complex flow physics, flow was computed about a simple configuration consisting of a delta planform with two jets in ground effect (Refs. 5-7). The experimental work of Paulson and Kemmerly[1] had indicated that the flow about this configuration produces much the same flow physics as the flow about even a very complex and realistic configuration, such as an F-18 in ground effect. The non-time-accurate simulations of flow past the delta wing showed the capability to capture jet impingement/entrainment, ground vortex formation, and the ability to predict lift loss in ground proximity.[5-7]

In the present paper, time-accurate simulations of both straight-and-level and descending flight profiles are presented. Both the mean and unsteady characteristics of these flows are analyzed. Of particular interest is the flow unsteadiness due to apparent instabilities in the jet and ground vortex structures. Analysis of lift coefficient and pressure histories and extensive flow visualization are used to develop an understanding of the relationship between the observed

forces on the delta wing and the flow dynamics.

3. COMPUTATIONAL MODEL

The computational model consists of a 60° delta wing in a free-stream Mach number of 0.064 (70 ft/sec), and chord length (31 in.) based Reynolds number of 1.2 million, in ground effect. The wing is equipped with two choked thrust reverser jets (diameter 0.6 in.) exiting from jet pipes at an angle of 45° to the delta wing and at NPR (nozzle pressure ratio) of 1.8. These geometrical and flow conditions correspond to the conditions in the wind-tunnel and VRF experiments used for the validation of this study. The computational model duplicates the wind-tunnel conditions for straight-and-level flight (Fig. 1). In the wind-tunnel simulations of the straight-and-

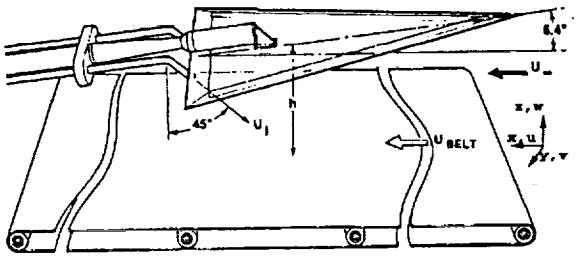

Fig. 1: The Wind-Tunnel setup.

level flight cases, the floor of the wind-tunnel is replaced by a moving belt to remove the boundary layer absent in flight tests. Identical procedure is followed in the computational model.

For the descent simulation there are some differences in the conditions between the computational model and the VRF experiment. In the VRF experiments, the delta wing is suspended from a cart that moves horizontally on rails, while the descent is simulated by the horizontal motion of the wing above a slanted ground board (Fig. 2). The VRF test sec-

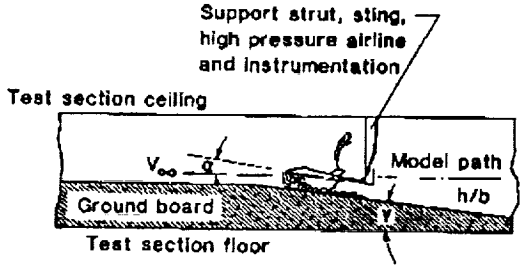

Fig. 2: The Vortex Research Facility setup.

tion is 150 ft. long. The ground board for the first 100 ft. of the test section is slanted upwards and the last 50 ft. is horizontal thus allowing simulation of descent followed by straight-and-level flight. In the computational model, the delta wing remains stationary and the free-stream moves over it, while the descent is simulated by moving the ground upwards. The ground grid is moved up at the effective experimental descent rate of Mach no. 0.004475 (4.9 ft/sec). For the descent simulations, the descent is started at $h/b = 1.0$ as opposed to the experimental starting height of $h/b = 2.0$ (where h is the height of the delta wing measured at two-thirds of the chord above the ground, and b is the wing span) to lower computational expense. The experimental data shows small differences between descending and straight-and-level lift coefficients at $h/b = 1.0$, indicating that there should be little difference between the static and dynamic flow structures at this height. Therefore, the descending case can be initialized using the flow field for straight-and-level flight at $h/b = 1.0$ without introducing significant errors.

3.1 Grids

The accuracy of the simulation of a complex flow problem, such as under study here, depends strongly upon the choice of grids. The straight-and-level flight simulations were performed using grids that would be extendible to the descent case. Body-conforming grids were generated about the delta wing, the jet pipe, and the ground to resolve the boundary-layers, and an overset "jet" grid was used to resolve the jet (Figs. 3, 4, 5). The mated delta-wing, jet, and pipe grids overset a ground grid. The overset topol-

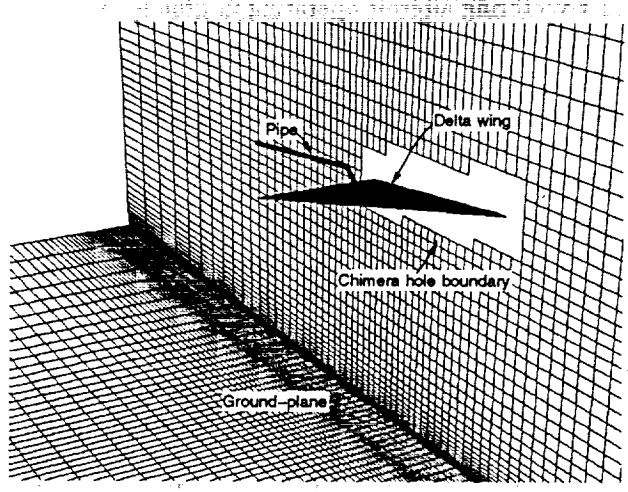

Fig. 3: The ground-plane grid.

ogy allows relative motion of component grids and thus efficiently manages grid points for moving-body simulations. It has been used in the past to simulate store separation[8] and the separation of the Solid Rocket Boosters from the Shuttle/Main Tank assembly.[9] Here, the descent is simulated by moving the ground grid in the upward direction. The data transfer between the grids is achieved using a new implementation[10] of a grid communication scheme referred to as the Chimera scheme.[11] Using this scheme, solutions are computed independently on all the grids. Overset/overlapping grids feel the influence of other grids via hole and outer boundaries. Hole

boundaries are artificial boundaries in grids. The solution is ignored on all points within a hole boundary as this area/volume is either overset by a solid body (hole made by delta wing in the ground and the jet grids), or it is resolved by a finer grid (hole made by the jet grid in the ground grid). In the straight-and-level flight computations, the interpolation coefficients required for grid communication at the outer and the hole boundaries are computed just once. However, for the descent simulation they have to be recomputed periodically due to the relative motion of grids.

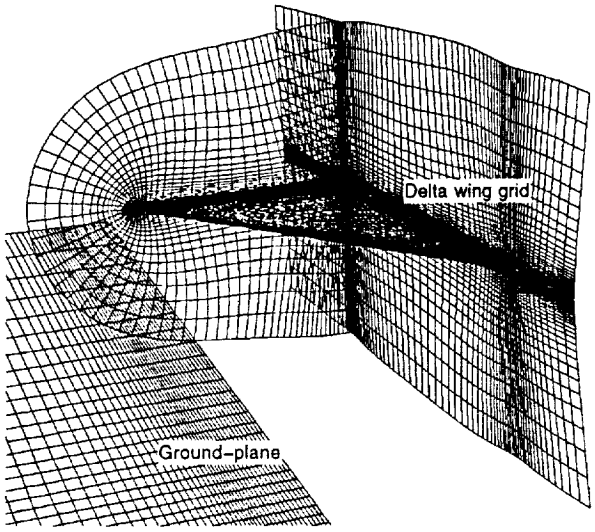

Fig. 4: The delta wing grid.

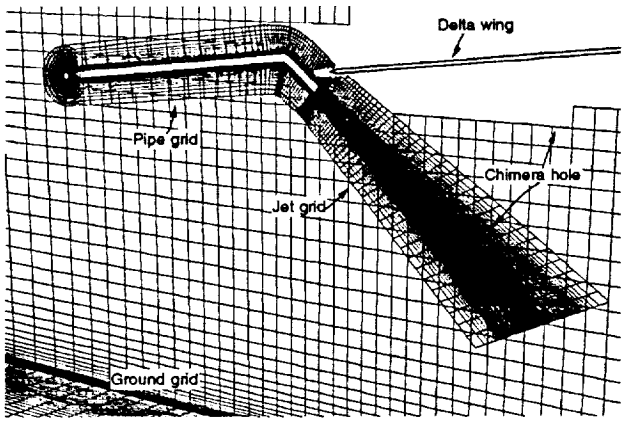

Fig. 5: The pipe and the jet grids.

3.2 Numerical Algorithm

Time-accurate computations were carried out on a Cray-YMP by solving the three-dimensional Navier-Stokes equations, using the OVERFLOW[12] code, on overset grids. Flow was computed on one half of the configuration with the assumption of symmetry about the x-z plane. The equations are discretized by using a diagonalized three-factor scheme,[13] which is second-order accurate in space, and at most first-order accurate in time. Higher-order time accuracy is possible by using subiterations. The code is used to solve the conventional dependent variable vector $[\rho, \rho u, \rho v, \rho w, e]^T$ where ρ is density, u, v, and w are Cartesian velocity components, and e is the total energy per unit volume. Speed of sound, delta wing centerline chord, free-stream density, and $\gamma \times$ pressure (γ is specific heat ratio for air) are used as reference quantities.

3.3 Boundary Conditions - Straight-and-level flight cases

Ground grid inflow and jet exit values are specified to match the wind-tunnel conditions. The ground plane moves at the same velocity as the free stream to remove the boundary layer effects. A no slip condition is used at the delta wing and pipe surfaces. On solid surfaces, density is extrapolated from one grid point away and pressure is computed by solving the normal momentum equation. All variables are extrapolated at the ground grid outflow plane.

3.4 Boundary Conditions - Descent cases

In the VRF experiments, the delta wing moved relative to the ground, however in these simulations the delta wing remains stationary and the free-stream moves over it. The inflow boundary conditions on the ground grid are specified to match the delta wing velocity (70 ft/sec), and sea-level density and pressure. Additionally, the co-ordinate transformation between the VRF setup and the computational model requires that the floor of the computational ground grid move at the same speed as the free-stream. All other boundary conditions are specified in a similar manner as for the straight-and-level flight cases.

4. RESULTS

4.1 Parametric Studies

Parametric computational studies were performed utilizing the straight-and-level flight setup to evaluate the effect of grid density. It was determined that the computed lift is a strong function of the jet trajectory. In turn, it was found that the jet trajectory can be heavily influenced by the level of grid refinement. It was found that no practical Cartesian ground plane grid could support the experimentally observed jet trajectory. Rather, the total jet momentum would decay rapidly with distance from the nozzle exit, and the jet would finally become so weak that it would be deflected downstream by the oncoming flow. This was in distinct disagreement with the experimental flow visualizations of Paulson.[1] It is for this reason that the jet grid was added to the computational model. With the jet grid, and low levels of spatial numerical dissipation, the jet penetrates far upstream, impacts the ground plane, and spreads to form a thin wall jet. The high speed and large surface area of the wall

jet result in significant flow entrainment. Because the entrained flow accelerates, a low static pressure region forms under the delta wing, and lift loss occurs. The results of these parametric studies were used to select the grid topology and density for all work presented here.

For the descent simulations, additional two-dimensional parametric studies were carried out to determine the effect of time step Δt on simulations involving moving grids by descending a two-dimensional center section of the delta wing in ground effect. It was shown that for a high value of Δt (1.0), the ground cushion effect may not be captured. For smaller time steps (Δt=0.5), the solution indicates increased lift with ground proximity based on conventional ground effect. Further reductions in time step indicate convergence of lift histories and do not show any new flow physics. In these simulations, a $\Delta t = 0.002$ is used due to stability considerations. The above study shows that the chosen time step is small enough to accurately capture the flow features in the descent simulation.

4.2 Test Case Studies

Visualizations of the flow about the delta wing at $h/b = 0.25$ and 1.0 for straight-and-level flight are presented in Plate 1. The instantaneous streamlines passing through the nozzle exit plane indicate that at $h/b = 1.0$ the jet does not have sufficient momentum to impact the ground. As a result, the level of flow entrainment is low and little lift loss is encountered. However, at $h/b = 0.25$ the jet does impact the ground and, as described above, significant flow entrainment occurs, a low pressure pocket forms under the delta wing, and significant lift loss is encountered. Because of the care taken in minimizing computational errors due to numerical dissipation and grid resolution, the predicted lift coefficients are in reasonable agreement with experimental data (Fig. 6).

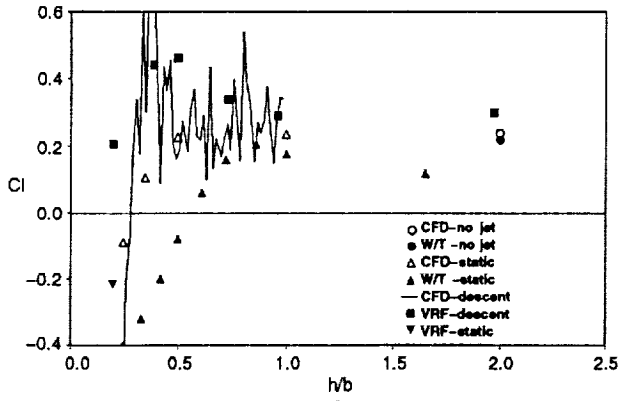

Fig. 6: Comparison between the experimental and computational C_l values.

The experimental values obtained from the VRF were smoothed by Paulson and Kemmerly (Ref. 14) following the procedure outlined in Fig. 7. The computed data presented in Fig. 6 for the descent case has been filtered so as to match the sampling rate of the experimental data. However, no smoothing procedure similar to the experimental procedure (Fig. 7) has been carried out.

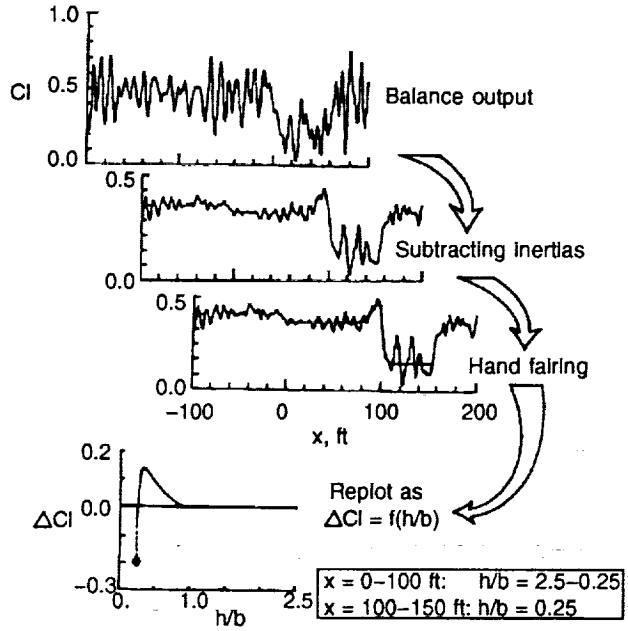

Fig. 7: VRF raw data processing.[14]

At higher heights above the ground, insignificant differences are observed between the straight-and-level flight and the descent cases. The gross flow features and mechanism of lift loss are same for both the cases. The descent lift curve indicates increased lift between $h/b = 0.5$ and 0.4 due to the conventional ground cushion effect. However as the delta wing approaches the ground, differences become apparent as indicated by higher value of C_l at $h/b = 0.35$ for the descent case as compared to the straight-and-level flight case.

The computed time histories of the lift-coefficient for both the straight-and-level flight at various heights above the ground (Fig. 8) and the descent case (Fig. 9) show large temporal variations and increased amplitude in lift oscillation with ground proximity. Preferred frequencies of these oscillations are

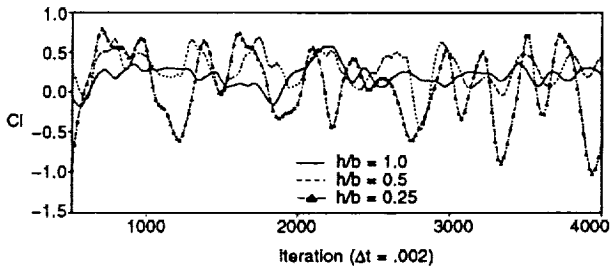

Fig. 8: The lift history of the straight-and-level flight cases.

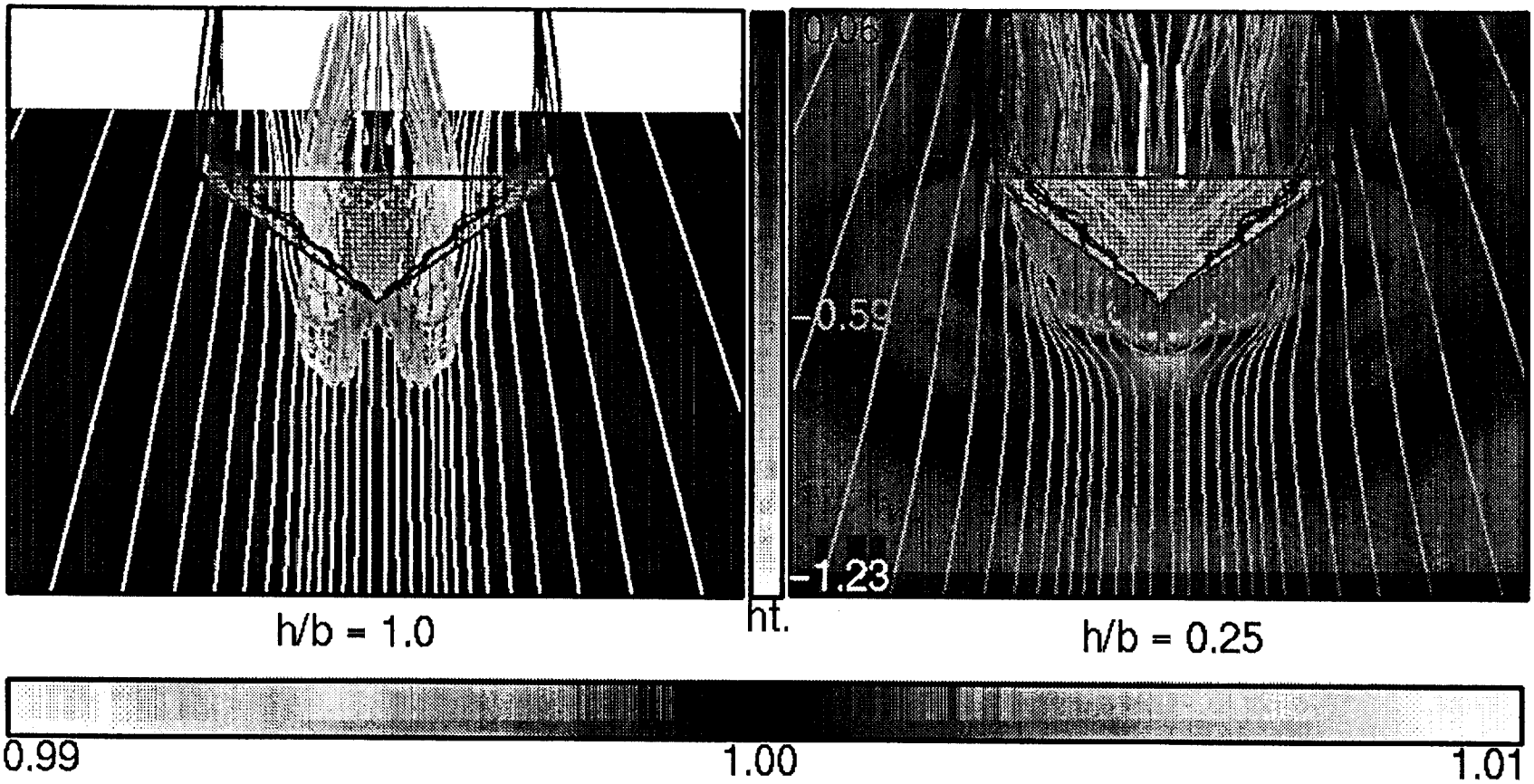

Particle traces shaded by height; ground shaded by normalized pressure.

Plate 1: Comparison of particle traces for straight-and-level flight.

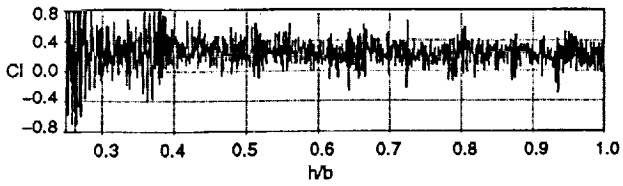

Fig. 9: Lift history of the descent case.

identified by computing power spectra of the time-varying lift histories (Fig. 10, 11). Power of all spectra presented in this work has been normalized using maximum power. For the descent case, the spectra are obtained over segments of descent (Fig. 11).

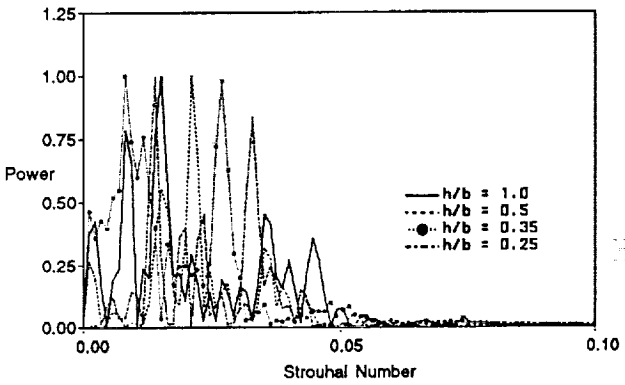

Fig. 10: Power spectra of lift history for the straight-and-level flight cases.

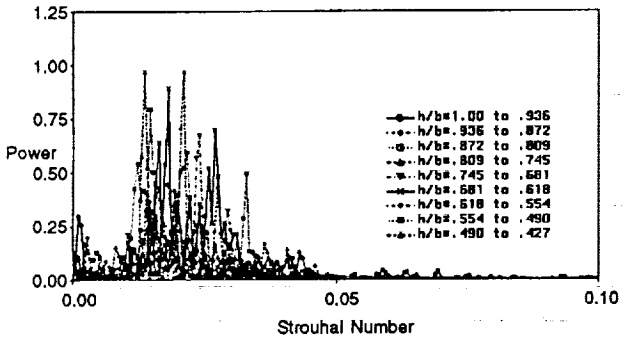

Fig. 11: Power spectra of lift history for the descent case.

These spectra indicate that preferred frequencies are confined in the narrow range of Strouhal number = 0.015 to 0.030. (St. = f Dj/Uj, where Dj and Uj are jet diameter and velocity respectively)

Flow visualizations indicate a number of flow features that could cause large temporal variations and increased amplitude in lift oscillation with ground proximity. For example, vortices shedding from the jet lip interact in non-periodic, almost random pairings; as a result the jet strength and trajectory vary with time. The jet oscillates both laterally, towards and away from the symmetry plane, and in the streamwise direction. There is also evidence of a complex Kármán vortex street shedding behind the dual jet configuration. Finally, the ground vortex height oscillates.

To determine if the ring vortex dynamics causes the observed variation in lift, temporal variations in pressure at the jet lip and four diameters downstream are analyzed (Fig. 12, 13). Power spectra of these pressure histories, presented in Fig. 14 indicate an initial shedding frequency of St. = 0.53 at the jet exit, dropping to a vortex passage frequency in the range of 0.1 to 0.2 by four diameters downstream. Although the initial shedding frequency is lower than the experimentally observed frequencies (probably due to the large time-step and inadequate grid resolution), the observed passage frequency (0.1 to 0.2) near the end of the potential core is within the range of experimentally observed ring vortex Strouhal numbers, as compiled by Gutmark.[15] The reduction in frequency as the probe is lowered from the jet lip to four diameters downstream is attributed to vortex pairings observed in flow visualizations. Because the range of observed frequencies due to the ring vortex dynamics is much higher than the observed time period in the lift variations, it is unlikely that the ring vortex structures are the dominant cause of the lift oscillations.

To determine if the lift oscillations are related to the lateral/streamwise jet oscillations, the temporal variation of the pressure field on the under surface

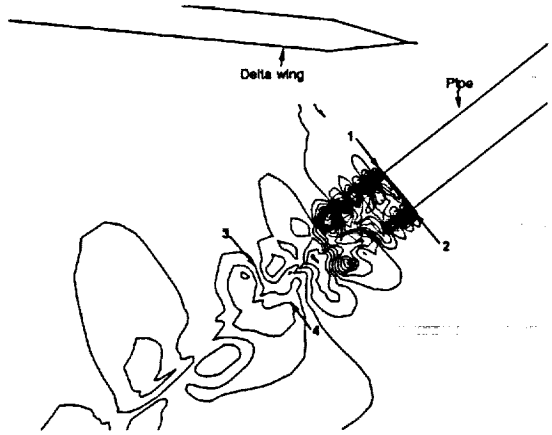

Fig. 12: Vortex shedding at the jet lip: Probe locations.

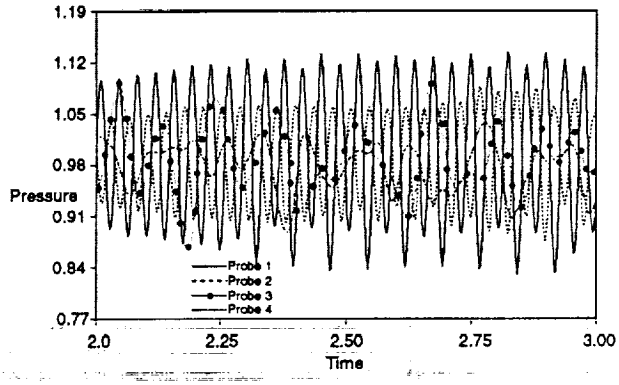

Fig. 13: Pressure samples at the jet probe locations.

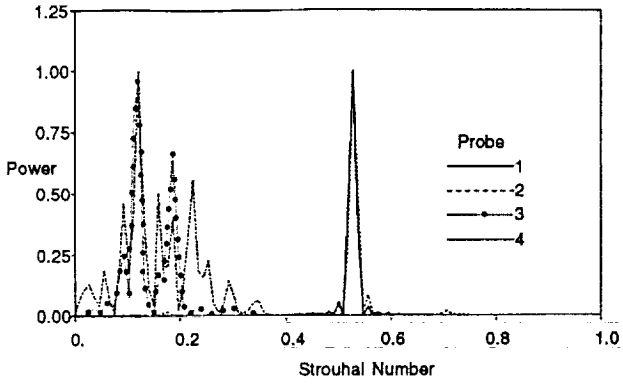

Fig. 14: Power spectra of pressure sampled at the jet probe locations.

of the delta wing is visualized. Concentric pressure waves emanating from the jet region move along the under-surface of the delta wing (Plate 2). Pressure distribution on the under-surface of the delta wing is shown at two different steps corresponding to instances when the under-surface is dominated by the high pressure and low pressure regions respectively of the pressure wave (Plate 2). Flow visualizations indicate that lift oscillates in synchrony with the movement of peaks (high-pressure) and troughs (low-pressure) of the pressure wave on the under-side of the delta wing. Based on this, it appears that the lift oscillations are related to these pressure waves. These waves are similar in shape and magnitude to the pressure waves observed on the ground plane (Plate 1) as well.

The history of the pressure variations at four points on the ground plane are presented in Fig. 15. These pressure histories were extracted as the delta wing descended through $h/b = 0.35$. Spectra analysis of

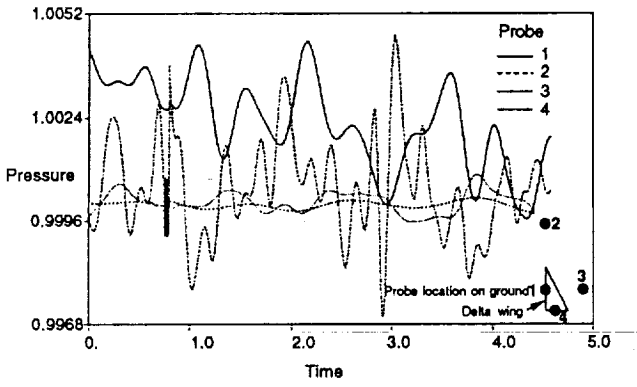

Fig. 15: Pressure samples at the ground probe locations.

these histories, presented in Fig. 16, show a preferred frequency of St. = 0.015, which is within the range of lift oscillation frequency. Because of this match in frequency, and the observation that the pressure waves only exist when the jets are present, and also they emanate from the jet vicinity, it appears that the lift oscillations are due to large scale motions of the jet and jet-induced flow structures.

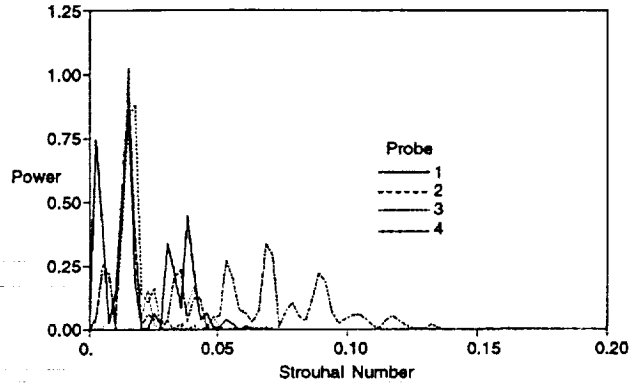

Fig. 16: Power spectra of pressure sampled at the ground probe locations.

The very low frequency ground vortex oscillations (St. = f Dj/Uj = 0.006) observed by Cimbala et. al.[17] suggest that lift oscillations could be related to ground vortex oscillations. These low-frequency oscillations, referred to as "ground vortex puffing," are caused when the ground vortex first grows and then, when it can no longer retain its structure, collapses. However, in these computations, the ground vortex appears only at lower heights (Fig. 17, 18), yet the same narrow range of low-level-frequency lift oscillations occur over the range of computed heights. For this reason, it appears the lift oscillations are not related to ground vortex puffing.

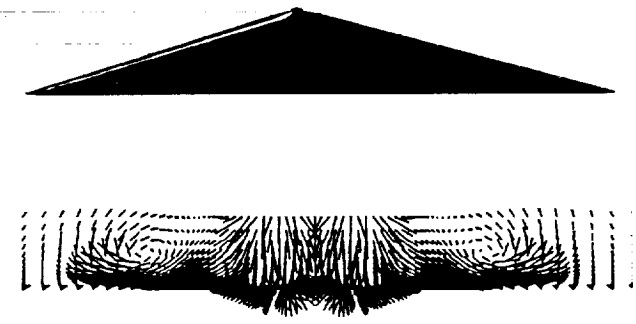

Fig. 17: Front view of the ground vortex.

There is evidence of a Kármán vortex street behind the dual jet. The frequency of this vortex street has yet to be determined, however, the shedding frequency for a Kármán vortex street for flow past a circular cylinder (jet in this case) for similar Reynolds numbers (jet-diameter-based) is in the range of St. = 0.18 to 0.20.[16] The computed lift oscillation frequency range corresponds to free-stream velocity based St. = 0.23 to 0.46. This frequency range is very close to the expected vortex street fre-

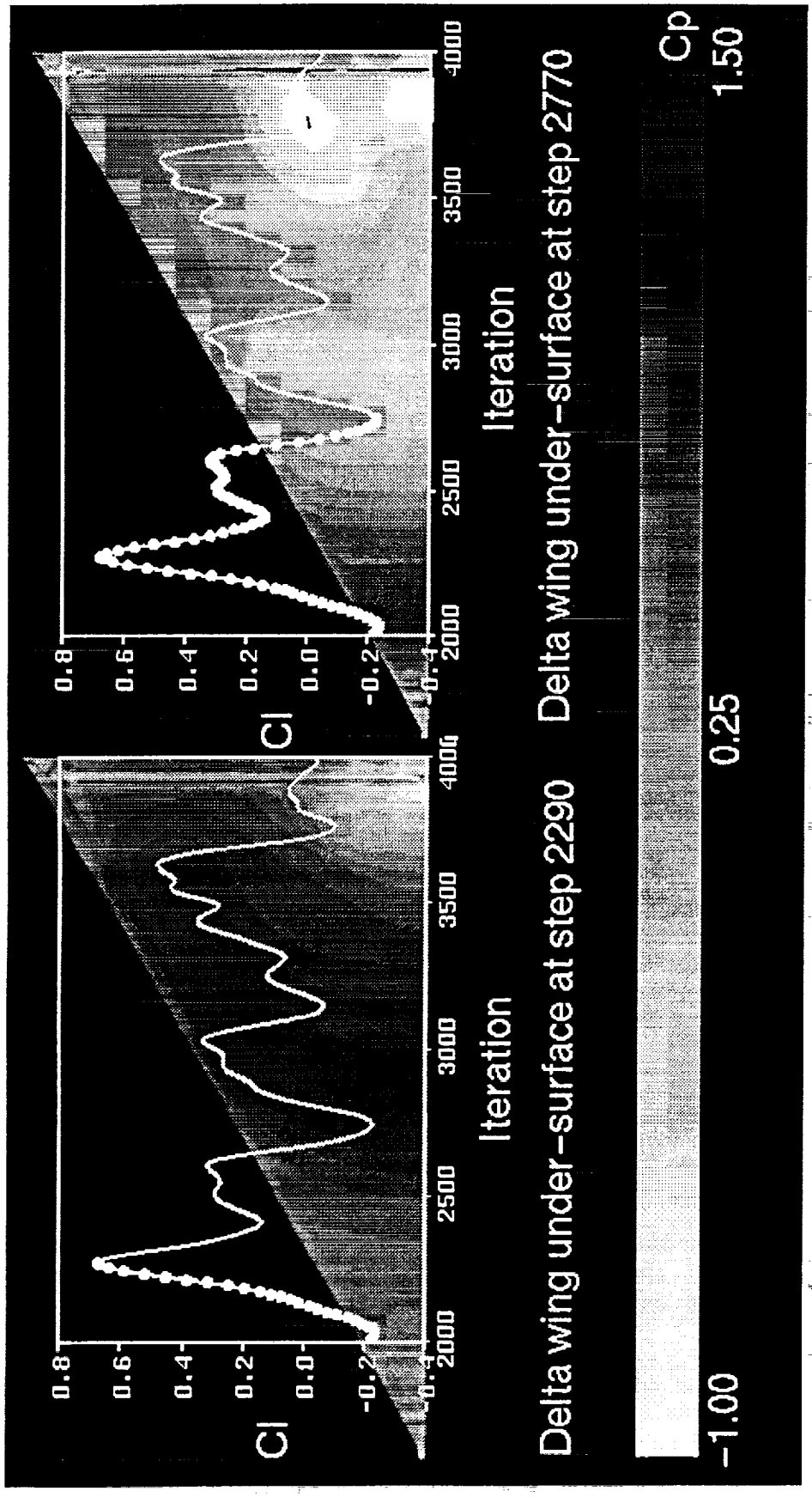

Plate 2: Correspondance of Cp and Cl oscillation at h/b = 0.35.

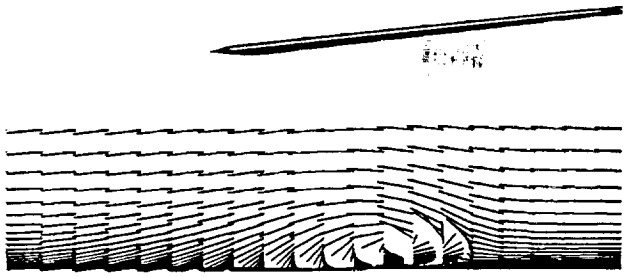

Fig. 18: Side view of the ground vortex.

quency. However, the position of the Kármán vortex street past the trailing edge of the delta wing makes it an unlikely feature that can affect the lift oscillations. Further, no correlation has been found between the wave-like nature of the pressure field on the under-surface of the delta wing and the Kármán vortex street.

The computational simulation captures the qualitative physics, as indicated by typical lift-coefficients at high h/b values and low lift-coefficient values at lower heights indicating suck-down (Fig. 6). Computed values fall within the data discrepancy band in the two experimental facilities (note C_l difference between the VRF and W/T results for $h/b = 1.0$ and $h/b = 0.25$). Quantitatively, the CFD simulation under-estimates the lift loss for straight-and-level flight cases. This could be due to the lack of a turbulence model in these simulations. Inclusion of a turbulence model would have increased the jet spreading and resulted in increased flow entrainment. No turbulence model was included in these simulations due to lack of a rational approach to apply an algebraic turbulence model to a flow of this complexity. A higher order two-equation model, for example a $k-\epsilon$ model, would have pushed the computational cost beyond what could be accommodated.

5. CONCLUSIONS

Lift loss in ground proximity, as may be encountered during STOL operations, was computed by solving flow past a delta wing with thrust reverser jets in the straight-and-level and descent flight profiles.

Efforts were made to minimize numerical errors due to grid resolution and time step. Overset grids were used to capture the jet trajectory. Two-dimensional parametric studies were carried out to determine the effect of time step Δt on simulations involving moving grids. The computed unsteady result (descent case) showed convergence for smaller values of Δt and indicates that for higher Δt, the ground cushion effect may not be captured. The time-step used in these simulations was sufficiently small to capture the descent related flow features.

The time-accurate computations for the straight-and-level flight were performed for a number of heights (h/b=1.0, 0.5, 0.35, and 0.25) above the ground. The computations over-predict the lift coefficient, however flow physics corresponding to lift loss with increased ground proximity is captured.

The time-accurate simulation of the descent from $h/b = 1.0$ to $h/b = 0.25$ captures the initial increased lift due to the conventional ground cushion effect followed by lift loss due to the suck-down effect as the delta wing approaches the ground. The computed lift coefficients are in fair agreement with the experimental values.

Both the straight-and-level flight and descent simulations exhibit high levels of unsteadiness. Spectra of the lift histories indicate preferred frequencies in the narrow range of St. = .015 to .03 for the straight-and-level flight over all computed heights. The same range of frequencies is preferred when spectra are computed over segments of the descent.

Efforts were made to understand the unsteady flow structures which produce the lift oscillations. The ring vortex shedding frequencies were deemed too high to cause the lift oscillations. Kármán vortex street was ruled out as the feature causing lift oscillations due to its position beyond the trailing edge of the delta wing. Further, no correlation could be found between the wave-like nature of the pressure distribution on the under-surface of the delta wing and the ground, and the vortex street.

Presence of a "wave-like" pressure field in the vicinity of the jet indicates that the jet oscillations result in moving pressure waves. It was shown that the lift oscillation frequency is related to the frequency of these waves. Analysis of the temporal variations of pressure at various locations on the ground indicated frequencies within the range of the lift oscillation frequencies. Based on this, it was concluded that the lift oscillations are due to large scale motions of the jet and jet-induced flow structures.

Ground vortex was ruled out as the cause of lift oscillations as it appears only at lower heights. Lift oscillations, however, over same range of preferred frequencies appear even at higher heights (e.g. $h/b = 1.0$). It is conjectured that ground-vortex-puffing type of flow physics occurs in the vortex formed behind the jet causing its size to oscillate, and resulting in lift oscillations.

6. References

[1] Paulson, J. W. and Kemmerly, G. T., "An Assessment of Ground Effects Determined by Static and Dynamic Testing Techniques," Ground Vortex Workshop, NASA Conference Publication 10008, NASA Ames Research Center, 1987.

[2] Van Dalsem, W. R., "Study of Jet in Ground Effect with Crossflow Using the Fortified Navier-Stokes Scheme," AIAA Paper 87-2279, 1987.

[3] Van Dalsem, W. R., Panaras, A. G., and Steger, J. L., "Numerical Investigation of a Jet in Ground Effect with a Crossflow," SAE Paper 872344, 1987.

[4] Stewart, V. R., Kuhn, R. E., and Walters, M. M., "Characteristics of the Ground Vortex Developed by Various V/STOL Jets at Forward Speed," AIAA Paper 83-2494, 1983.

[5] Chawla, K., Van Dalsem, W. R., and Rao, K. V., "Simulation of a Delta Wing with Two Jets in Ground Effect," Computing Systems in Engineering, **1**, pp. 483-494, 1990.

[6] Chawla, K., Van Dalsem, W. R., and Rao, K. V., "Numerical Study of a Delta Planform with Multiple Jets in Ground Effect," SAE Paper 892283, 1989. Also in SAE 1989 Transactions, Journal of Aerospace, Section I, pp. 1555-1567.

[7] Chawla, K., Van Dalsem, W. R., and Rao, K.V., "Simulation and Analysis of a Delta Planform with Multiple Jets in Ground Effect," AIAA Paper 90-0299, 1990.

[8] Dougherty, F. C. and Kuan, J. H., "Transonic Store Separation Using a Three-Dimensional Chimera Grid Scheme," AIAA Paper 89-0637, 1989.

[9] Meakin, R. L. and Suhs, N. E., "Unsteady Aerodynamic Simulation of Multiple Bodies in Relative Motion," AIAA Paper 89-1996, 1989.

[10] Meakin, R. L., "A New Method for Establishing Inter-Grid Communication among Systems of Overset Grids," AIAA Paper 91-1586, 1991.

[11] Benek, J. A., Buning, P. G., and Steger, J. L., "A 3-D Chimera Grid Embedding Technique," AIAA Paper 85-1523, 1985.

[12] Buning, P. G. and Chan, W. M., "OVERFLOW/F3D User's Manual," NASA Internal Memorandum, NASA Ames Research Center, Moffett Field, CA, March 1991.

[13] Pulliam, T. H. and Chaussee, D. S., "A Diagnol Form of an Implicit Approximate Factorization Algorithm," Journal of Computational Physics **39**, pp. 347-363, 1981.

[14] Kemmerly, G. T. and Paulson, J. W., "Investigation of a Moving-Model Technique for Measuring Ground Effects," NASA Technical Memorandum 4080, January 1989.

[15] Gutmark, E. and Ho, C. M., "Preferred Modes and the Spreading Rates of Jets," Physics of Fluids, **26**, pp. 2932-2938, 1983.

[16] Schlichting, H., Boundary Layer Theory, McGraw Hill Book Company, pp. 32, 1979.

[17] Cimbala, J. M., Billet, M. L., and Gaublomme, D. P., "Experiments on the Unsteadiness Associated with a Ground Vortex," Journal of Aircraft, 28, No. 4, pp. 261-267, 1991.

Appendix II

PREV. ANN

93A22617

AIAA 93-0197
Tracking Flow Features Using Overset Grids

K. Chawla
MCAT Institute
NASA Ames Research Center
Moffett Field, CA

and

D. W. Banks
University of California
Davis, CA

31st Aerospace Sciences Meeting & Exhibit
January 11-14, 1993 / Reno, NV

TRACKING FLOW FEATURES USING OVERSET GRIDS

Kalpana Chawla*
MCAT Institute
NASA Ames Research Center
Moffett Field, CA
and
David W. Banks†
University of California at Davis
Davis, CA

Abstract

A method is proposed to use overset grid topology to track dynamic flow features. Features of interest such as moving shock waves and vortices are overset with relatively fine tracker grids. Solutions are computed on the various grids and information is exchanged at intergrid boundaries. A grid track-sensor variable such as pressure is used to track the position of the flow feature to be resolved. The tracker grid is moved to the position where the track-sensor variable has the desired value (generally a maximum or a minimum) and new interpolation coefficients are computed for information exchange across grid boundaries. Solutions are computed at the current location and time-step, and grid motion is brought into the solution via time metrics. The method is demonstrated by tracking a moving shock and vortices shed behind a circular cylinder. It is conjectured that the method would show significant benefits in resolving features such as wakes behind oscillating airfoils and trajectories of jets issuing from rotating nozzles as encountered during thrust-vectoring.

Introduction

Engineering Computational Fluid Dynamics (CFD) simulations routinely require the use of adaption procedures to resolve flow fields of interest by providing denser grids in areas of high gradients. The existing methods can be classified into two approaches. In the first approach, new grid points are added in the regions of high gradients, and in the second approach grid points are moved to cluster in the regions of high gradients.

In the adaptive mesh refinement technique, regions of the global grid are refined, and re-refined to provide additional points so as to resolve the flow gradients accurately.[1] This approach seems to be well suited for problems with moving flow features. However, generally, explicit methods are used in conjunction with this approach, thus inhibiting the time-step size. This approach has been exploited efficiently in conjunction with unstructured grids where explicit approaches are more efficient.[2]

Grid movement based adaption methods are more popular in the structured-grid arena. The points are moved either 1) based on minimization of some error measure or 2) based on a measure of artificial forces acting between nodes.[3]

The error measures in the minimization method are computed, amongst other approaches, using modified equation analysis. In modified equation analysis, the discrete equations are expanded using Taylor series to obtain the original differential equation plus error terms. The grid is then adapted to minimize the truncation error terms. Truncation error based measures have been used successfully to adapt grids to moving shocks.[4]

Methods utilizing artificial forces to move grid points make use of, amongst other approaches, the spring analogy. In the methods utilizing spring analogy, it is imagined that the grid points are connected to each other with springs and that flow variables to which the grid is adapted are equivalent to forces acting at grid points. Equations are formulated so that a uniform spring force distribution is achieved. This approach has been used to solve complex three-

*Research Scientist, Member AIAA.
†Research Assistant, Member AIAA.

dimensional flows.[5,6] A number of variants of this method exist and the reader is referred to Ref. 3 for more details on this and other adaption methods.

Most of the structured-grid based adaption methods require that once the grid has been adapted, the solution be updated on the adapted grid by an interpolation method. For problems requiring time-accurate analysis, subiterations have to be carried out as the interpolated solution is not necessarily a solution of the governing equations. Alternatively, time metrics may be used to obtain solution on the deformed (adapted) grid. Flow fields consisting of dynamic features do not lend themselves very well to this adaption procedure. Frequent grid adaptions are required as the flow features move around. Further, adaption to flow variables generally results in grids of poor quality. Modified equation analysis indicates that grids with skewed, high stretching and high aspect ratio cells may result in solution errors.[4] As a result, grids that have been adapted to solution variables, now, in addition, have to be adapted to grid quality functions such as skewness, straightness, and orthogonality as well.[7] The adaption problem with these constraints may be very stiff, and may not converge.

In this paper, a method is proposed to adapt the static flow features such as wall jets and shear layers via conventional adaption methods, and tracking the dynamic flow features such as vortices and moving shocks by using dynamic overset grids, termed "tracker grids" here. Overset grids have been used successfully in the past to provide grid enrichment in regions of high gradients to resolve jets[8,9], and to resolve shear layers and wake flows[10]. The grid densities used in these overset grid examples to resolve static flow features were determined based on parametric studies. Sample two-dimensional problems were solved to determine grid densities that would provide desired resolution of frequencies and flow features. The structured grids used were solved implicitly allowing for the corresponding benefits of large time-step size. Fig. 1, for example, shows a result from the simulation of a delta wing with thrust-reverser jets in ground effect.[8,11] Particle traces starting at the jet

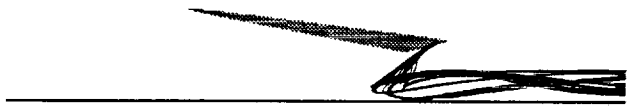

Fig. 1: Jet trajectory without an overset grid.

exit in Fig. 1 do not reach the ground. However, when the solution is obtained with an additional overset grid (Fig. 2) to resolve the jet, the jet is able to reach the ground (Fig. 3). The engineering requirement of this simulation is to predict correct air-loads on the delta

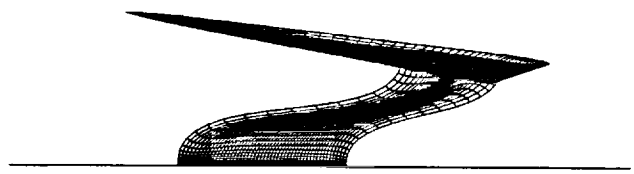

Fig. 2: An overset grid to resolve the jet.

wing, which is possible if the jet trajectory is simulated correctly. The overset grid is just fine enough to allow correct prediction of jet trajectory and hence air-loads, but too coarse to simulate unnecessary features such as modes of jet deformation.

Fig. 3: Jet trajectory with an overset grid.

In the present study, overset grids are used to resolve large, distinct, dynamic flow features such as moving shocks and vortices by oversetting the relatively coarse background and component grids with finer grids; thus allowing grid enrichment in the regions of high gradients. These grids are then used to track the dynamic flow features. It is conjectured that the proposed approach will show promise in tracking flow features associated with bodies in motion, e.g., wakes behind oscillating airfoils and trajectories of jets issuing from rotating nozzles as encountered during thrust-vectoring.

Approach

Tracker Grid Motion Procedure:

The approach to track the flow features is very similar to the simulation of moving bodies using overset grid technology.[12,13] First, the problem is solved on the global and component grids. Then Cartesian tracker grids are introduced at locations where the chosen track steering variable, or its gradient (termed "sensor variable" here) has the minimum or maximum value. Centroids of these grids are placed exactly over locations where sensor variables have desired values. The solutions on the tracker grids are initially interpolated from the solution in the existing domain. The flow solution is then carried out on all the grids for a few steps so that the solutions on the tracker grids match the solutions on the underlying grids. After this, solution is computed for a desired number of time steps, and a search is initiated at the centroid of the tracker grid. A stencil-walk from this location leads

to the new position where the sensor variable has the local maximum/minimum value. This new position is written to a file which is then read by a grid communication package to determine new interpolation coefficients for transferring solutions at grid hole and outer boundaries. Holes are regions within which the solution is not computed. The region within the hole boundary is either overset by a solid body or a finer grid. Once the intergrid communication process has been completed, the solution process is begun once again. Time metrics are used to bring the effect of grid motion into the solution. The above-mentioned procedure is summarized in Fig. 4.

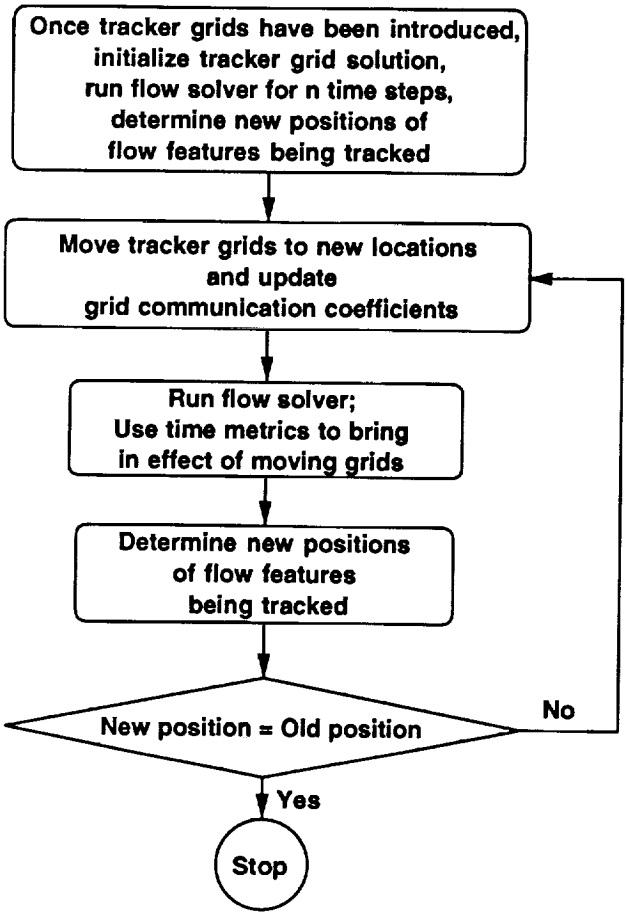

Fig. 4: Tracking procedure.

Tracker Grid Type:

The choice of Cartesian or analytically defined tracker grids offers a number of advantages, however tracker grids are not limited to this family alone. Since the nature of the flow feature is generally not known a priori, a Cartesian grid would be the simplest choice. Not only are the grid quality issues absent with this choice, but also Cartesian flow solvers could be used to obtain solutions on these grids at relatively cheaper costs.[14] In the proposed simulation, one could use 1) a global Cartesian background grid, 2) curvilinear component grids to resolve boundary layers and implement turbulence models, and 3) Cartesian tracker grids to follow the dynamic flow features.

Other advantages of choosing Cartesian tracker grids include:

1) Cartesian grids would lend themselves to grid refinement much more easily, if it was desired to relate the grid density to a rigorous error measure as opposed to parametric studies. Techniques such as Richardson's extrapolation to perform grid-sensitivity studies could be carried out relatively easily.

2) Search routines to locate the sensor variable's maxima/minima are simple and inexpensive on these grids.

3) Once a grid family is chosen, advance knowledge of the size of the grid can be used to ensure that tracker grids do not come closer than a certain distance (which would imply a waste of points).

4) In other scenarios, the size of the grid helps in specifying minimum overlap that must exist between two tracker grids. Without this specification, the holes caused by tracker grids may not overlap, resulting in global grid field points between tracker grids as shown in Fig. 5.

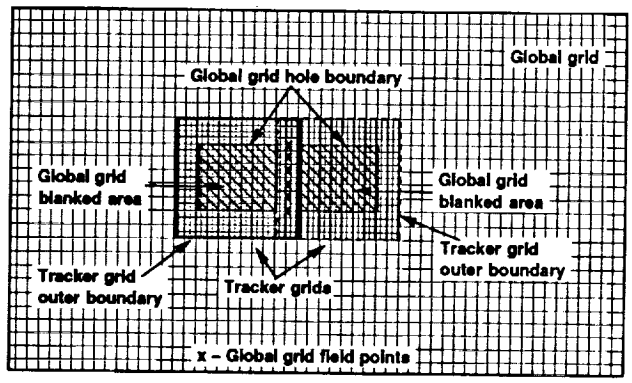

Fig. 5: Insufficient overlap between tracker grids.

Track Sensor Variable:

The choice of the sensor variable to track the flow feature is problem-dependent. For example, pressure gradient may be chosen as the sensor variable for a moving shock. One should choose variables that are representative of the features that need to be resolved. These variables should offer a wide variation in values with the surrounding flow field so that they have distinct minima or maxima on the tracker grids to enable accurate tracking. Flow fields with very small flow features or dynamic features with weak gradients scattered all over may not be suitable for this tracking approach.

Errors:

The most common errors associated with overset grids occur when a fine grid transfers a large flow gra-

dient onto a coarse grid. These errors can be minimized by ensuring that flow gradients are small at intergrid boundaries if grid densities of communicating grids are widely different. If large gradients exist at the intergrid boundaries, then both the global and the overset grid should be capable of resolving the gradient at that location. This is generally ensured by providing grids of similar densities. For example, shear-layer studies of Ref. 10 carried out on overset grids indicate that it is possible to simulate unsteady flow features accurately on static overset grids, suggesting that once proper attention is paid to positions and densities of grids, space-conservation errors are probably minimal.

Time-conservation error studies of Ref. 15, for moving grids, show that a small phase error can occur in the solution. If all grid communication boundaries are updated at the end of a solution step, some of this error may diminish. For global space-time related conservation errors associated with overset grids, the reader is referred to Ref. 16. Rigorous analysis of conservation errors associated with overset grids is in progress at NASA Ames.

Examples

The motivational problem for tracking flow features using overset grids is the simulation of a descending delta wing with thrust reverser jets in ground environment.[13] When the delta wing is more than one wing span above the ground, the thrust reverser jets do not strike the ground. Instead, the free-stream causes the jets to move downstream. However, as the delta wing approaches the ground, the jet trajectory starts to change. At heights of about one-half wing span above the ground, the jet is able to strike the ground and spreads into a thin wall jet that can be resolved properly by the fine grids used in the vicinity of the ground to resolve boundary layers. In an ideal scenario, one would require only the grid in the jet vicinity to be refined so as to predict correct jet trajectory, as opposed to using a fine background grid that could be computationally expensive. In the proposed approach, one grid would be introduced in the jet vicinity at the beginning of the simulation. After the jet has developed in this grid, other tracker grids would be added so that the jet trajectory could develop in these grids. This problem is deemed too complicated to test the tracking method; instead simpler demonstration problems are tested and discussed below.

Validation Cases

Two demonstration problems, namely tracking a shock, and tracking a vortex are used for validating the tracking procedure. Past experience indicates that a large number of engineering problems require finer grids in regions of the computed domain to yield solutions of desired accuracy. However, in both of these problems, grid arrangements are chosen such that only the tracking procedure is validated. No effort is made to demonstrate solutions of higher accuracy with the use of tracker grids. For the shock problem, validation will be successful if the shock is tracked at the correct shock speed. The shock speed is known a priori as it is the solution of the analytical problem corresponding to the specified initial conditions. For the vortex tracking problem, the tracking procedure is started after the vortex is positioned more than a diameter downstream of the cylinder. The method will be validated if it can be shown that tracking does not change the vortex shedding rate and the relative positions of the vortices.

The Moving Shock Problem

An initial condition corresponding to a shock speed of Mach number of 2.81 was prescribed on a Cartesian grid. A fine Cartesian grid was introduced at the shock position. Fig. 6 shows the background Cartesian grid and the boundary of the overset, fine, shock-tracker grid. The location of the left-moving shock is

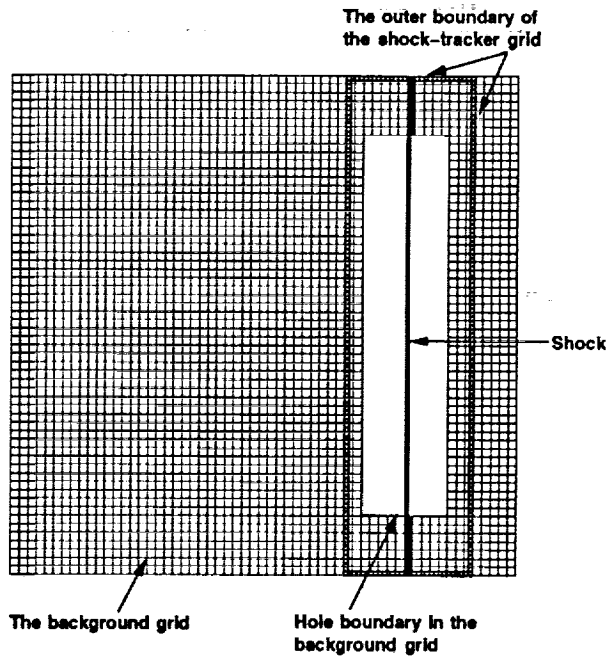

Fig. 6: The grid setup for the left moving shock

shown by the vertical thick solid line passing through the blanked area of the background grid. Interpolation coefficients for grid communication across the two grids were obtained using Domain Connectivity Function (DCF).[17] OVERFLOW,[18] a flow solver, was then used to obtain the solution on this grid arrangement for ten time steps. Finally, a new routine

in the program was used to determine the location of the highest pressure gradient in the fine tracker grid. The location of the tracker grid is stored in a file and used by DCF to generate new interpolation coefficient files. The flow solver was then run again, and the time metrics were computed so that effect of grid motion could be brought into the solution. Figure 7 shows the location of the moving shock (pressure jump) and also the location of the tracker (solid line) and background grids (dashed line). It can be seen that the tracker grid is able to follow the moving shock automatically. The computed shock speed with and without tracker

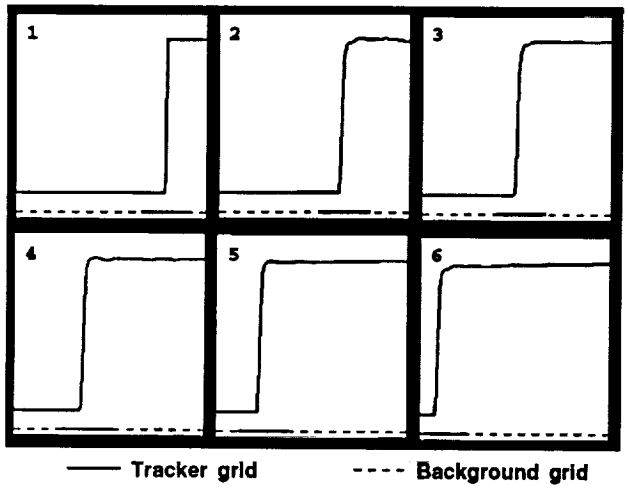

Fig. 7: A tracker grid following a shock.

grid matches the analytical shock speed. Comparison of shock positions with and without tracker grids is shown in Fig. 8. It should be pointed out that shocks

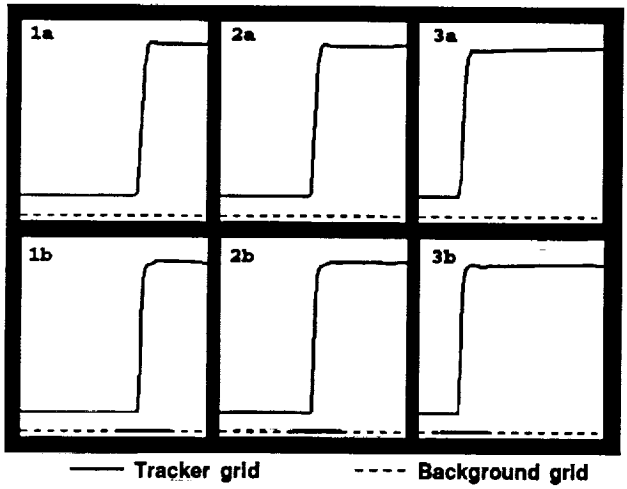

Fig. 8: Shock speed comparison without (1-3a) and with (1-3b) tracker grid.

of speeds as low as Mach 0.06 were tracked correctly using this procedure. The low shock speed cases are important because they allow the errors to accumulate over longer lengths of time and show the effect of errors more clearly.

Flow Past a Circular Cylinder

The previous example is essentially a one dimensional dynamic flow feature. In this example, two-dimensional features, namely vortices behind a circular cylinder, are tracked. A similar procedure as described above is followed, however, now the sensor used to position the tracker grid is vorticity. The tracker grid is searched for maximum vorticity after the solution has been carried out for some time-steps, and then moved to this new location. Figure 9 shows the grid setup for this case consisting of a background Cartesian grid, a body-conforming grid around the cylinder and a Cartesian tracker grid. Fig. 10 shows

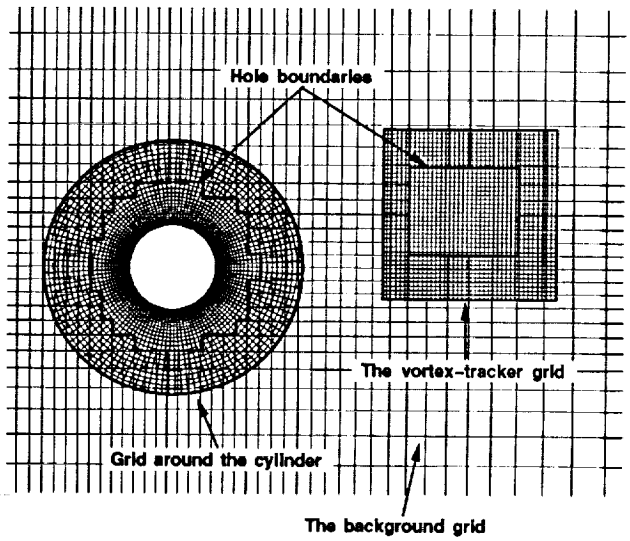

Fig. 9: The grid setup for vortex tracking.

vorticity contours at a Reynolds number of 200, and the tracker grid position as it follows a vortex. The results with and without tracker grid are similar, indicating that Strouhal number is not affected with this approach.

Another case was tried by tracking two vortices, yielding very similar results, as shown in Fig. 11. The positions of the vortices, and thus the Strouhal number, are almost identical to the one tracker grid case. This problem is a motivation for developing automatic introduction and removal of grids. Grids could be removed when the associated gradients have weakened such that the global grid can resolve them.

Conclusions

The overset grid methodology has been successfully used to track one-dimensional and two-dimensional flow features in time and space. It is expected that the

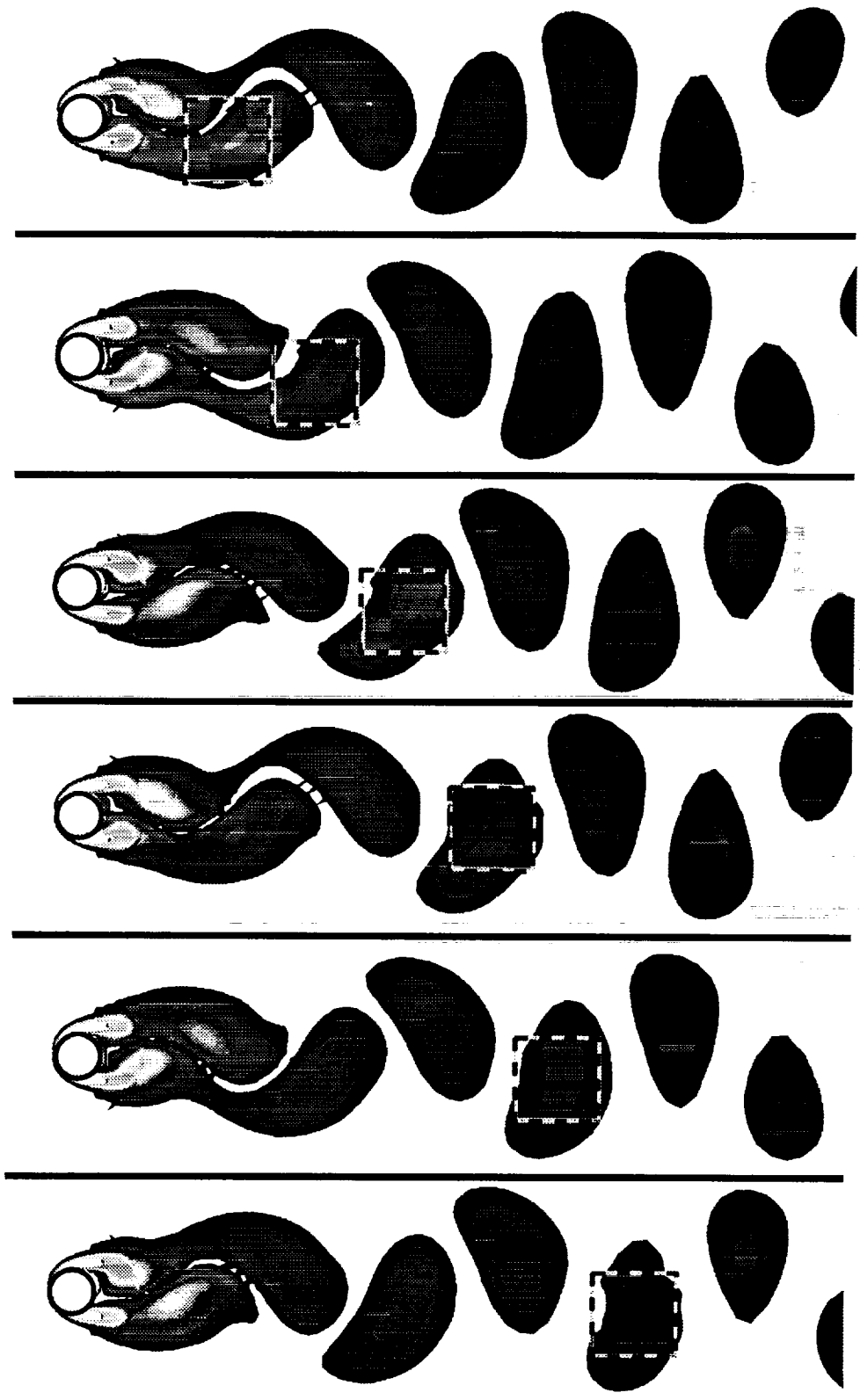

Fig. 10: Vorticity contours (white = large vorticity, black = small vorticity) for flow past a circular cylinder at a Reynolds number of 200 showing a tracker grid following a vortex.

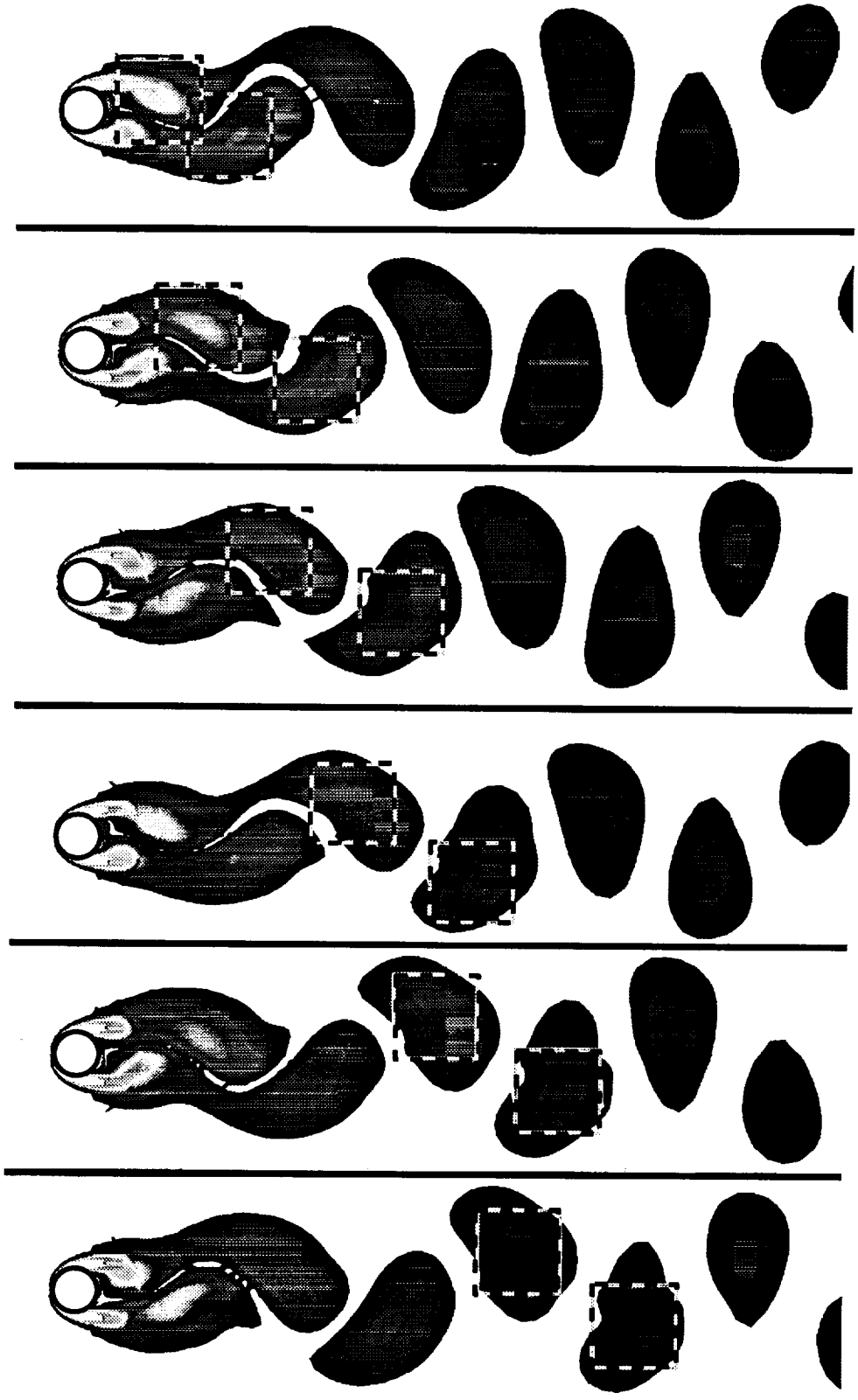

Fig. 11: Vorticity contours (white = large vorticity, black = small vorticity) for flow past a circular cylinder at a Reynolds number of 200 showing tracker grids following two vortices.

tracking approach will minimize grid-quality-related solution errors by allowing Cartesian tracker grids to track flow features as opposed to deforming the grid to meet the same objective.

This approach uses tools very similar to those used in overset moving body simulations. Solutions are computed on the various grids and information is exchanged at various boundaries. A sensor variable such as pressure is used to track the position of the flow feature to be resolved. The tracker grid is moved to the position where the sensor variable has the desired value (generally a maximum or a minimum) and new interpolation coefficients are computed for information exchange across grid boundaries. Solutions are computed at the current tracker locations and time-step, while grid motion is brought into the solution via time metrics. The method is demonstrated by tracking a moving shock, and vortices shed behind a circular cylinder.

The grid steering is automated at this stage as illustrated by the examples shown. Work is in progress to automate the process of introduction and removal of tracker grids. It is conjectured that the method would show significant benefits in resolving features such as wakes behind oscillating airfoils and trajectories of jets issuing from rotating nozzles as encountered during thrust-vectoring.

Future Work

A strategy is being formulated to introduce and remove tracker grids automatically. Tracker grids will be discarded once global grid density is sufficient to resolve the flow gradient. A method may be developed to change the size of the tracker grids based on the value of the gradient they are trying to resolve. Also, a method may be evaluated to track flow features based on error estimates. The new methodologies will be tested on analytic/simple two-dimensional problems initially. Once the method has matured, it will be applied to a realistic three-dimensional problem.

References

[1] Berger, M. J. and Colella, P., "Local Adaptive Mesh Refinement for Shock Hydrodynamics," Journal of Computational Physics, Vol. 82, pp. 64-84, May 1989.

[2] Mavriplis, D. J., "Accurate Multigrid Solution of the Euler Equations on Unstructured and Adaptive Meshes," AIAA Journal, Vol. 28, No. 2, pp. 213-221, 1990.

[3] Hawken, D. F., "Review of Adaptive-Grid Techniques for Solution of Partial Differential Equations," Progress in Aerospace Sciences, Vol. 24, pp. 29-49, 1987.

[4] Klopfer, G. H. and McRae, D. S., "The Nonlinear Modified Equation Approach to Analyzing Finite Difference Schemes," AIAA Paper 81-1029, 1981.

[5] Djomehri, M. J. and Deiwert, G. S., "Solution Adaptive Program SADAP3D," AIAA Paper 91-2903, 1991.

[6] Davies, C. B. and Venkatapathy, E., "A Simplified Self-Adaptive Grid Method, SAGE," NASA-TM-102198, 1989.

[7] Lee, K. D. and Loellbach, J. M., "A Mapping Technique for Solution Adaptive Grid Control," AIAA 89-2178-CP, 1989.

[8] Chawla, K., Van Dalsem, W. R., and Rao, K.V., "Simulation and Analysis of a Delta Planform with Multiple Jets in Ground Effect," AIAA Paper 90-0299, 1990.

[9] Smith, M., Chawla, K., and Van Dalsem, W., "Numerical Simulation of a Complete Aircraft in Ground Effect," AIAA Paper 91-3293, 1991.

[10] Atwood, C. A. and Van Dalsem, W. R., "Flowfield Simulation about the SOFIA Airborne Observatory," AIAA Paper 92-0656, 1992.

[11] Chawla, K., Van Dalsem, W. R., and Rao, K.V., "Simulation of a Delta Wing with Two Jets in Ground Effect," Computing Systems in Engineering, Vol. 1, Nos 2-4, pp. 483-494, 1990.

[12] Meakin, R. L., "Unsteady Aerodynamic Simulation of Multiple Bodies in Relative Motion," AIAA Paper 89-1996, 1989.

[13] Chawla, K. and Van Dalsem, W. R., "Numerical Simulation of STOL Operations Using Thrust Reversers," AIAA Paper 92-4254, 1992.

[14] Joseph L. Steger, private communication.

[15] Dougherty, F. C. and Kuan, J. H., "Transonic Store Separation Using a Three Dimensional Chimera Grid Scheme," AIAA Paper 89-0637, 1989.

[16] Steger, J. L., "Chimera Simulation of Viscous and Vortical Flows about Aircraft," Appendix-1, Matrix Analysis, IBM CFD Short Course, April 29 to May 3, 1991.

[17] Meakin, R. L., "A New Method for Establishing Inter-Grid Communication among Systems of Overset Grids," AIAA Paper 91-1586, 1991.

[18] Buning, P. G., Chan, W. M. et. al., "OVERFLOW/F3D User's Manual," NASA Internal Memorandum, NASA Ames Research Center, Moffett Field, CA, March 1991.

Appendix III

Color Illustration